TC34 of ISSMGE, International Workshop on Deformation of Earth Materials
May23, 2001, Sendai, Japan

DEFORMATION AND FAILURE CHARACTERISTICS OF RECTANGULAR CLAY SPECIMENS DURING TRIAXIAL COMPRESSION

F. Oka, T. Kodaka and T. Takyu
Department of Civil Engineering, Kyoto University, Kyoto 606-8501, Japan

Abstract

In order to grasp deformation and failure behaviors of clay under 3-D condition as well as large deformation and strain localization, a series of triaxial compression tests using rectangular clay specimens with different heights and width are conducted. To use the rectangular specimen is convenient for this object. Shear strain distribution localized with compression is also successfully observed by taking digital photograph from two sides of rectangular specimens and image analysis of their digital photograph. It is found that the bifurcation phenomena, e.g. formation and progress of various shear planes, failure with buckling, unstable behavior in the stress – strain relationships, can be clearly observed in the present tests.

Introduction

Clarification and predictions of strain localization of geomaterials are indispensable research topics to improve an accuracy of computation of the geotechnical engineering problems. Most of past numerical studies concerning the strain localization have been done under the plane strain conditions (e.g. Yatomi et al. 1989, Oka et al. 1994, Asaoka and Noda 1995, Oka et al 1996, Asaoka et al. 1997a, Asaoka et al. 1997b, Oka et al. 1997, Oka et al. 2001) and most of experimental researches are done by the triaxial tests using cylindrical specimen (e.g. Ikeda and Goto 1993, Asaoka et al. 1997a, Asaoka et al. 1997b) or by the plane strain tests (Yoshida et al. 1994, Yoshida and Tatsuoka 1997). Nowadays, three-dimensional numerical analysis becomes actual computational tool not only for research works but also for design works. With respect to the strain localization in the ground, large difference between two- and three-dimensional analyses exists. It is necessary to analyze ground under three-dimensional condition to consider the shear band formation. In the present study, in order to grasp the deformation and failure behaviors of geomaterials as true three-dimensional phenomena, the triaxial compression test using the rectangular clay specimen was conducted. By using the rectangular specimen, it is easy to set up the boundary conditions in the three-dimensional computation work. In addition, since a transverse section of specimen does not have many axis of symmetry compared with the cylindrical specimen, it is relatively easy to observe the strain localization. The distribution of shear strain observed in side of specimen can be obtained by the image analysis of digital photographs.

Test Program

The used clay is Kyoto Fujinomori Clay (w_L=62%, I_p=33%, G_s=2.69g/cm3). Normally consolidated clay sample that was prepared by remolding and then pre-consolidation was trimmed to be rectangular shape. The shapes of specimens in each case are illustrated in Table 1 and Figure 1. The specimens were isotropically consolidated to 200 kPa (cell pressure 400 kPa and back pressure 200 kPa), and then subjected to a standard undrained compression test. The stress – strain relationship of soil specimen was measured by load cell and LVDT. To obtain local shear strain distributions observed in a side of specimen, a digital camera took the photographs of side surface of specimen, which were drawn 2mm meshes, and then the image analysis in the digital photographs was done.

Table 1 Test cases

Specimen No.		Rate of axial displacement	Rate of axial strain	Scale (cm)
A	1,2,3	0.08mm/min	0.067%/min	4×4×12
	4	0.12mm/min	0.1%/min	
	5	1.2mm/min	1%/min	
	6	0.012mm/min	0.01%/min	
B	1,2,3	0.08mm/min	0.1%/min	4×4×8
	4	0.08mm/min	0.1%/min	
C	1,2	0.08mm/min	0.1%/min	4×2×8
	3	0.08mm/min	0.1%/min	
D	1,2	0.08mm/min	0.2%/min	4×4×4
	3	0.04mm/min	0.1%/min	

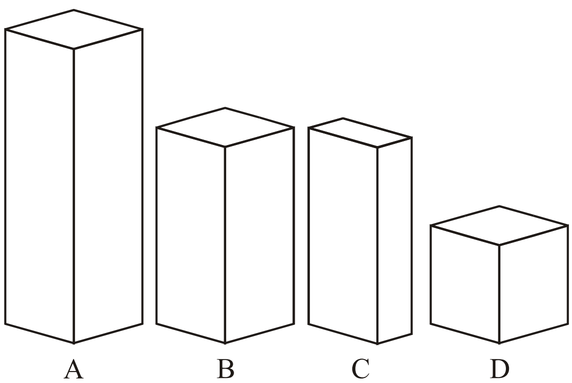

Figure 1 Shapes of rectangular clay specimens

Test Results

Effect of shape of specimens

In order to compare the test results by the various shapes of specimens, the test results from the constant axial strain rate tests (A-4, B-4, C-3 and D-3) and the constant axial displacement tests (A-1, B-3, C-2 and D-1) are shown in this secion. Figure 2 shows the stress – strain relationships obtained by the constant axial strain rate tests. The initial tangent of stress – strain curve of D-3 that is shortest specimen case is rather small compared with the other cases. Even though an axial strain rate is same, an actual axial loading speed of the shortest specimen is half or one third of that of longer specimens. Therefore it seems to occur the loading rate dependency behavior of clay. Although the peak strengths are almost same among three specimens except C-3, the slenderer specimen shows the smaller residual strength. Figure 3 shows the stress – strain relationships obtained by the constant axial displacement rate tests. The difference of initial tangent cannot be observed in these test cases. Tendency of the peak and residual strengths is similar to Figure 2. The rapid decreases of deviator stress are observed from the slenderer specimens cases A-1 and C-2. Figure 4 shows the shear strain distributions obtained by the image analysis of digital photographs. Both A-1 and C-2 show the buckling type failure mode. They show the unstable behavior in stress – strain curves compared with B-3 and D-1, which are observed the X pattern shear bands. The shorter specimen shows the more complex failure mode among the same sectional shape cases A-1, B-3 and D-1. Two shear planes occur without intersection in A-1 case. In the case of B-3, at least four shear planes crossing each other can be observed.

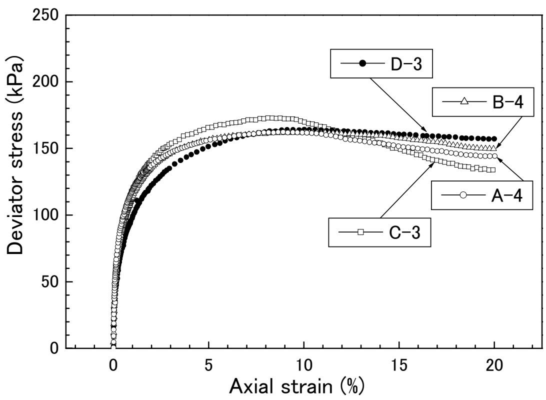

Figure 2 Stress-strain curves of constant axial strain rate tests
($\dot{\varepsilon}_a = 0.1\%/\mathrm{min.}$)

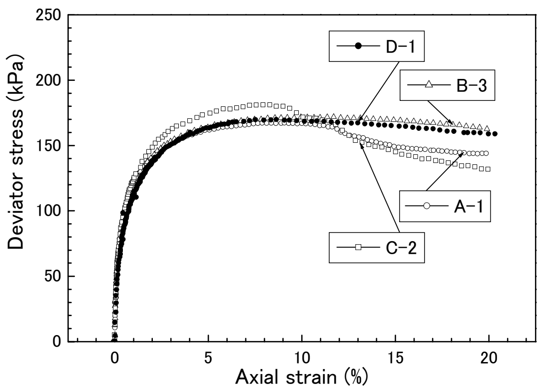

Figure 3 Stress-strain curves of constant axial displacement rate tests
($\dot{d}_a = 0.08mm/\mathrm{min.}$)

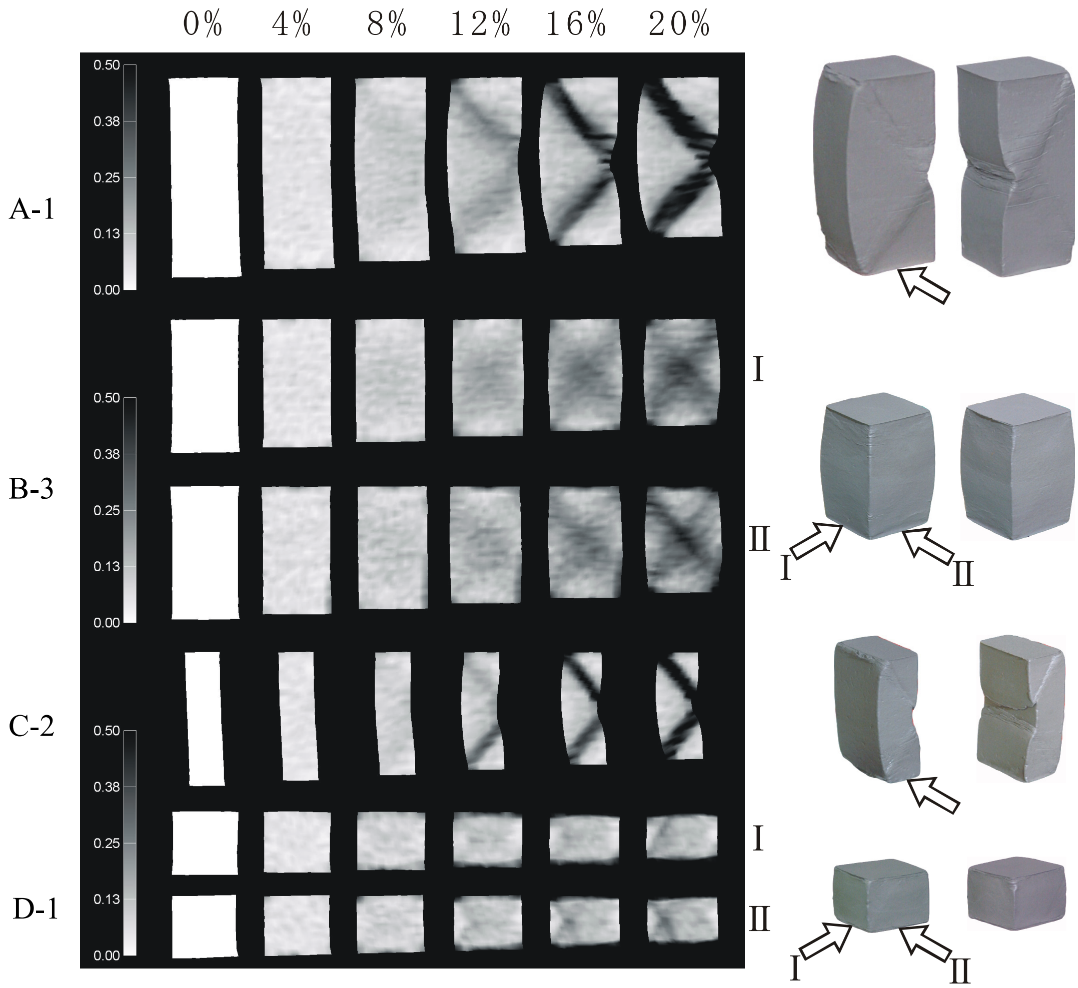

Figure 4 Shear strain distributions obtained by the image analysis

Effect of axial loading rate

In this section, only specimen A is used to investigate the effect of loading rate on failure mechanism of rectangular clay specimen. Figure 5 shows the stress – strain curves observed with three different axial strain rates. The local shear strain distributions obtained by the image analysis in digital photograph with different axial strain levels are shown in Figure 6 as well as the photograph of specimens after testing. In 8 and 12% axial strains, more contrasty distributions are also illustrated. Shear planes are clearly observed in any specimens and the local shear strain exceeds 100% near the shear plane. Although there is no difference in shear strain distributions among three specimens in small axial strain level, the difference in stress – strain relationships are clearly observed as shown in Figure 5. In the initial part of stress - strain curve, the fastest case, i.e. A-5, shows largest deviator stress among three cases. This tendency agrees with a traditional theory of time effect of clay. After the peak strength, however, the deviator stress of A-5 rapidly decreases to be the smallest residual strength. The decrease of deviator stress of A-5 is more significant than the other cases. It seems to be due to the buckling failure mode of the fastest loading case. In the slowest loading rate case, i.e. A-6, two shear planes cut through the specimen crossing each other. In the middle loading rate case, i.e. A-4, although the failure mode is similar to A-5, the thickness of the shear band is larger and the degree of localization seem to be smaller than that of A-5.

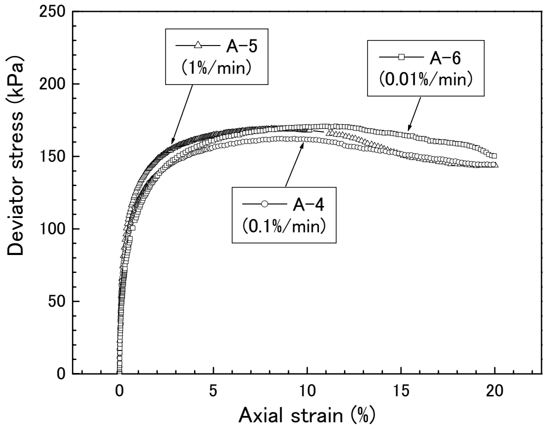

Figure 5 Stress – strain relationships (A-4, A-5 and A-6)

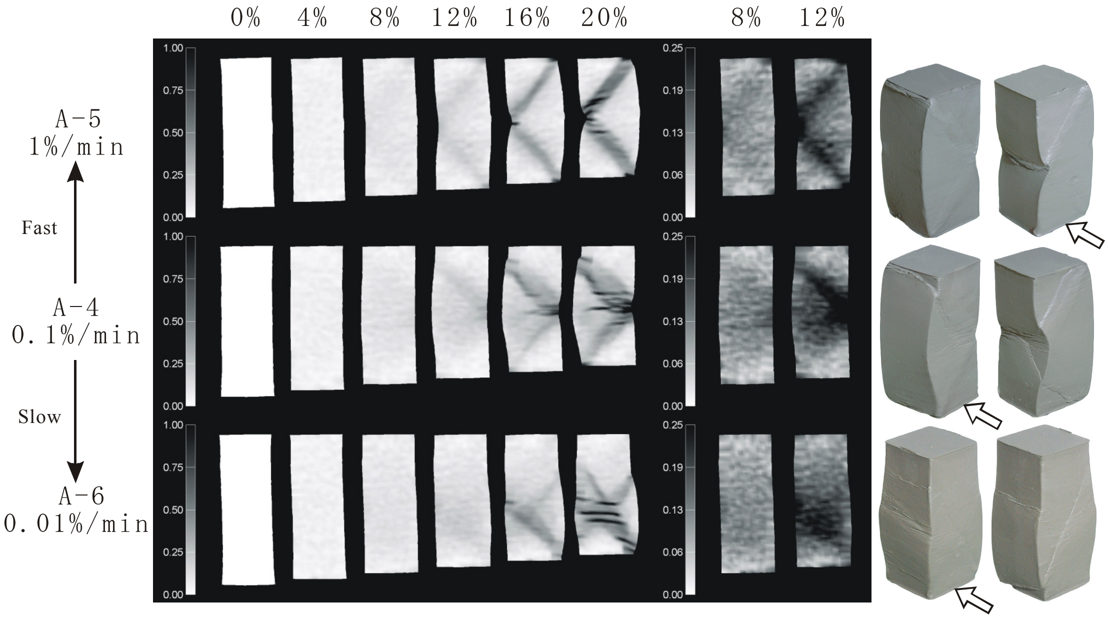

Figure 6 Shear strain distributions with different axial strain levels (A-4, A-5 and A-6)

Figure 7 shows the stress – strain relationships obtained by the same loading speed cases, A-1, A-2 and A-3 ($\dot{\varepsilon}_a = 0.067$%/min). In this figure, the stress – strain curves of A-4, A-5 and A-6 are also illustrated by solid lines to compare. In the small axial strain range less than 1%, the stress – strain relationships of A-1, 2 and 3 are similar to that of A-4, which is the closest loading rate ($\dot{\varepsilon}_a = 0.1\%$ /min). In the axial strain range over 1%, however, the difference of stress – strain relations occurs in three cases. The deviator stress of A-1 rapidly decreases around 12% axial strain. At that time, the shear band exceeding 25% shear strain can be observed as shown in Figure 8. The shear band formation seems to occur from around 8% axial strain. In the case of A-2 and A-3, however, the shear band formation cannot be observed in that axial strain level. In particular in the case of A-3, the clear decrease of deviator stress cannot be observed. Although the failure mode of A-3 is the buckling pattern that is similar to cases A-1 and A-2, the X patterned shear bands also occur in the bottom of specimen. The stress – strain curves of A-1 and A-3 bifurcate at around 7.5% axial strain, which corresponds to the strain level the localization can be clearly observed in A-1.

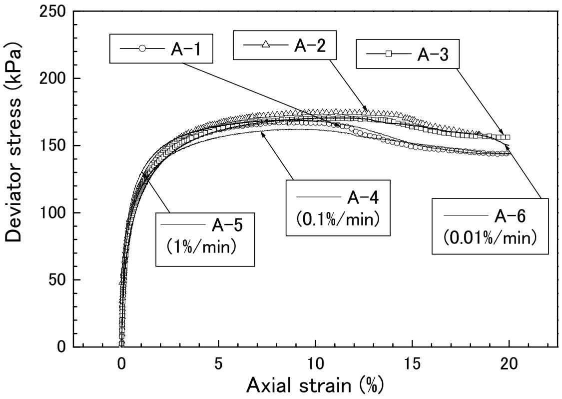

Figure 7 Stress – strain relationships (A-1, A-2 and A-3)

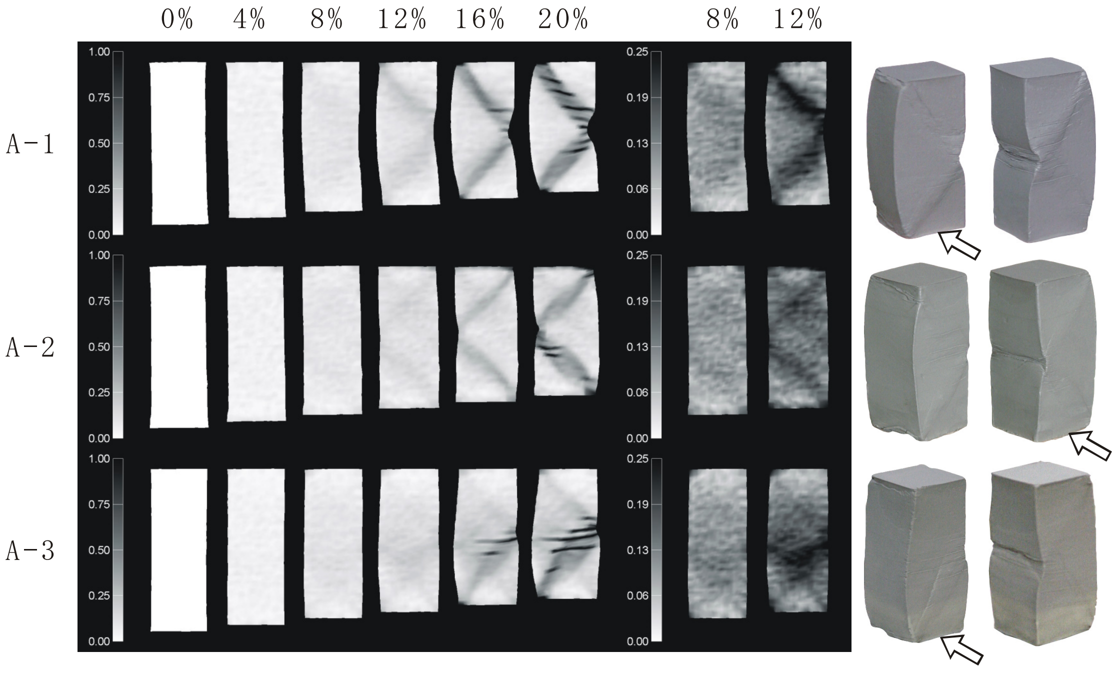

Figure 8 Shear strain distributions with different axial strain levels (A-1, A-2 and A-3)

Conclusions

In the present study, triaxial compression tests using rectangular clay specimen with different height and sectional shapes are conducted to discuss the three-dimensional failure behavior of clay. The local shear strain distributions are measured by the image analysis in digital photograph taken on a side surface of specimen during the triaxial compression test. The results obtained are as follows.

1) Shear planes are clearly observed in any specimens and the local shear strain exceeds 100% near the shear plane.

2) In the same loading rate tests, slenderer specimen shows more unstable behavior in the stress – strain relationships. The observed failure mode of the slender specimen looks likes buckling of column. More complex shear failure patterns are observed in the shorter specimens case, in which stress – strain relationships is more stable.

3) Even though the slender specimen is used, the X pattern shear bands are observed in the case of slow loading rate. According to the failure modes that occur in specimens, the stability of ultimate failure load fluctuates. Slower case shows more stable behavior due to the failure mode without buckling.

4) Different failure modes can be observed under the same test conditions, i.e. same loading rate and same shape of specimen. In that case, the axial strain level is so large that the localized shear strain occurs. Due to the various patterns of localization, the failure mode seems to change (so-called mode switching).

Discussion of large deformation and failure behavior using the slender specimen cannot directly link to the practical problem. It is, however, very important that the minute observation of the typical strain localizations in the specimen to improve the accuracy of prediction of progressive failure in numerical computation.

References

Asaoka, A. & Noda, T. 1995. Imperfection-sensitive bifurcation of Cam-clay under plane strain compression with undrained boundaries. Soil and Foundations 35(1): 83-100.

Asaoka, A., Nakano, M., Noda, T. & Kaneda, K. 1997a. Undrained creep rupture of normally consolidated clay triggered by the “mode switching” during pore water migration. In A. Asaoka, T. Adachi & F. Oka (eds), Deformation and Progressive Failure in Geomechanics; Proc. Intern. Symp., Nagoya, 1997: 21- 26. Pergamon.

Asaoka, A., Nakano, M., Noda, T., Takaine, T & Kaneda, K. 1997b. Progressive failure of heavily overconsolidated clay under constant load application, an experiment and its simulation. In A. Asaoka, T. Adachi & F. Oka (eds), Deformation and Progressive Failure in Geomechanics; Proc. Intern. Symp., Nagoya, 1997: 69 - 74. Pergamon.

Ikeda, K & Goto, S. 1993. Imperfection sensitivity for size effect of granular materials. Soils and Foundations 33(2): 157 - 170.

Oka. F, Adachi, T. & Yashima, A. 1994. Instability of an elasto-viscoplastic constitutive model for clay and strain localization. Mechanics and Materials 18: 119 - 129.

Oka. F, Adachi, T. & Yashima, A. 1996. A strain localization analysis using a viscoplastic softening model for clay. Intern. Jour. Plasticity 11(5): 523 - 545.

Oka. F, Yashima, A., Sawada, K & Adachi, T. 1997. Effect of viscoplas-tic strain gradient on strain localization analysis. In A. Asaoka, T. Adachi & F. Oka (eds), Deformation and Progressive Failure in Geomechanics; Proc. Intern. Symp., Nagoya, 1997: 27 - 32. Pergamon.

Oka, F., Jiang, M. & Higo, Y. 2001. Gradient dependent viscoplastic constitutive models and strain localization analysis of water satu-rated cohesive soil. In Desai et al. (eds.). Computer Methods and Advances in Geomechanics, Proc. Intern. Symp. Tuson. 2001: 519 – 524.

Yatomi, C., Yashima, A., Iizuka, A. & Sano, I. 1989. General theory of shear band formation by a non-coaxial CAM-CLAY model. Soils and Foundations 29(3): 41 – 53.

Yoshida, T., Tatsuoka, F., Siddiquee, M.S.A., Kamegai, Y. & Park, C.-S. 1994. Shear banding in sand in plane strain compression. In Chambon et al. (eds.). Proc 3rd Intern. Workshop on Localization and Bifurcation Theory for Soils and Rocks, Grenoble, 1994: 165 – 179.

Yoshida, T. & Tatsuoka, F. 1997. Deformation properties of shear band subjected to plane strain compression and its relation to particle characteristics. Proc. 14th ICSMGE. Humburg 1: 237 - 240.